JGR

The Canary Basin contribution to the seasonal cycle of the Atlantic Meridional Overturning Circulation at 26°N

M. D. Pérez-Hernández[1,2], G. D. McCarthy[3], P. Vélez-Belchí[4], D. A. Smeed[3], E. Fraile-Nuez[4], and A. Hernández-Guerra[1]

[1]Instituto de Oceanografía y Cambio Global (IOCAG), Universidad de Las Palmas de Gran Canaria, Las Palmas, Spain, [2]Department of Physical Oceanography, Woods Hole Oceanographic Institution, Woods Hole, Massachusetts, USA, [3]National Oceanography Centre, University of Southampton Waterfront Campus, Southampton, UK, [4]Centro Oceanográfico de Canarias, Instituto Español de Oceanografía, Santa Cruz de Tenerife, Spain

Abstract This study examines the seasonal cycle of the Atlantic Meridional Overturning Circulation (AMOC) and its eastern boundary contributions. The cycle has a magnitude of 6 Sv, as measured by the RAPID/MOCHA/WBTS project array at 26°N, which is driven largely by the eastern boundary. The eastern boundary variations are explored in the context of the regional circulation around the Canary Islands. There is a 3 month lag between maximum wind forcing and the largest eastern boundary transports, which is explained in terms of a model for Rossby wave generated at the eastern boundary. Two dynamic processes take place through the Lanzarote Passage (LP) in fall: the recirculation of the Canary Current and the northward flow of the Intermediate Poleward Undercurrent. In contrast, during the remaining seasons the transport through the LP is southward due to the Canary Upwelling Current. These processes are linked to the seasonal cycle of the AMOC.

1. Introduction

The Atlantic Meridional Overturning Circulation (AMOC) is a system of currents carrying warm shallow water northward and cold deep water southward. It carries 90% of the 1.25 PW (1 PW $= 10^{15}$ W) of ocean heat transport in the subtropical North Atlantic [*Johns et al.*, 2010; *McCarthy et al.*, 2015]. About 1 PW of heat is released to the atmosphere between 26°N and 50°N, which contributes to the relatively mild climate of northwest Europe. The RAPID/MOCHA/WBTS project (hereafter referred to as the RAPID array) is a joint UK/US project that has been delivering twice daily estimates of AMOC strength at 26°N since 2004 [*Cunningham et al.*, 2007] (Figure 1). The measurements have influenced our understanding of the variability of the AMOC in the North Atlantic from subannual [*Cunningham et al.*, 2007], interannual [*McCarthy et al.*, 2012] to multiyear [*Smeed et al.*, 2013] timescales.

The eastern boundary measurements of the 26°N array are located south of the Canary Islands, near the passage between Africa and Lanzarote (the so-called Lanzarote Passage (LP)) (Figure 1). The Canary basin is characterized by two different dynamical processes: the equatorward Canary Current (CC) that dominates the broad scale flow [*Hernández-Guerra et al.*, 2005; *Fraile-Nuez et al.*, 2010; *Pérez-Hernández et al.*, 2013] and the eastern boundary upwelling regime [*Mittelstaedt*, 1983; *Barton*, 1989]. The CC has been studied extensively in recent years with expandable bathythermograph [*Hernández-Guerra et al.*, 2002], moored observations [*Fraile-Nuez et al.*, 2010] and dedicated hydrographic programs: CANIGO [*Machín et al.*, 2006], CORICA [*Hernández-Guerra et al.*, 2005], ORCA [*Pérez-Hernández et al.*, 2013] and currently with ongoing projects RAPROCAN [*Vélez-Belchí et al.*, 2015] and SEVACAN. Both the CC and the upwelling regime transport North Atlantic Central Water (NACW) [*Hernández-Guerra et al.*, 2001; *Pérez-Hernández et al.*, 2013]. The CC evolves from the Azores Current and has a mean strength of 3.0 ± 1.0 Sv (1 Sv $= 10^6$ m³ s⁻¹) [*Comas-Rodríguez et al.*, 2011; *Pérez-Hernández et al.*, 2013]. The strength of the CC varies seasonally, carrying its weakest southward flux through the Canary Islands in winter, strengthening southward through the spring and summer before moving offshore and reaching its maximum southward flow in fall [*Machín et al.*, 2006; *Pérez-Hernández et al.*, 2013].

The flow in the LP also displays strong seasonality. Due to its proximity to the African shelf, the surface layers of the LP are influenced by the upwelling that occurs along the African coast. The upwelling jet called
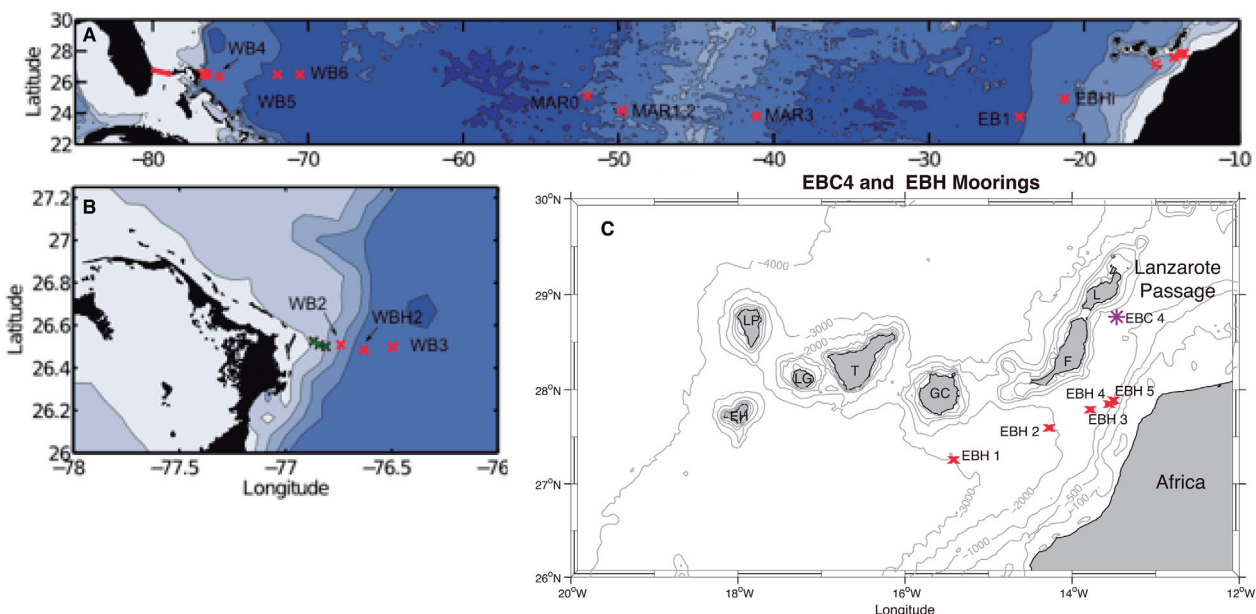
Figure 1. (a) The location of the whole RAPID array. (b) Amplified area of the western moorings (both are figures from *McCarthy et al.* [2015]). (c) Geographical study area and the location of the eastern moorings of the RAPID array (referred to as the EBH array), and the Eastern Boundary Current 4 (EBC4) mooring. The letters on the islands indicate their corresponding names: La Palma (LP), El Hierro (EH), La Gomera (LG), Tenerife (T), Gran Canaria (GC), Fuerteventura (F) and Lanzarote (L). The Lanzarote Passage refers to the channel between the islands of Fuerteventura and Lanzarote and the African coast. Dynamic height (red crosses) and current meter (green crosses) moorings from the RAPID array are shown together with the EBC4 current meter mooring (purple asterisk) and with the cable measurements of the Gulf Stream in the Florida Straits (red line).

Canary Upwelling Current (CUC) flows southward, parallel to the African shelf through the LP, during spring and summer, when the trade winds are intense [*Pelegrí et al.*, 1997, 2005; *Machín et al.*, 2006]. In contrast, in September and October the CUC becomes unstable and no longer flows near the coast [*Pelegrí et al.*, 2005; *Machín et al.*, 2006]. During this time of the year the flow through the LP surface layers reverses [*Hernández-Guerra et al.*, 2003; *Fraile-Nuez et al.*, 2010]. This reversal occurs at a time when the winds have decreased considerably and when the CC is on its westernmost position [*Pérez-Hernández et al.*, 2013]. The northward surface flow that occurs in fall in the LP in the thermocline layer is described as a partial recirculation of the CC in several studies [*Pelegrí et al.*, 2005; *Machín and Pelegrí*, 2006; *Laiz et al.*, 2012].

In the LP and along the African shelf an Intermediate Poleward Undercurrent (IPUC) around 1000 m has been found [*Hernández-Guerra et al.*, 2005; *Machín and Pelegrí*, 2009; *Machín et al.*, 2010]. The intermediate waters surrounding the Canary archipelago are a mixture of Mediterranean Water (MW) and Antarctic Intermediate Water (AAIW) [*Machín et al.*, 2010; *Fraile-Nuez et al.*, 2010]. When the IPUC is strongest to the north, the proportion of AAIW in the region increases [*Hernández-Guerra et al.*, 2003; *Pérez-Hernández et al.*, 2013]. The IPUC is not linked with the nearby upwelling, but with a remote forcing from the tropical North Atlantic [*Machín and Pelegrí*, 2009]. Intense Ekman pumping localized near the tropical African coast elevates the upper isoneutrals, stretching the intermediate water column. Due to conservation of potential vorticity, this results in more northward flow. The IPUC appears from summer to mid-fall [*Fraile-Nuez et al.*, 2010].

The Canary Islands are tall volcanic islands that constitute a barrier for the predominantly northeasterly winds that blow parallel to the African coast. They generate cyclonic (anticyclonic) wind cells on their west flank (east flank) downstream [*Jiménez et al.*, 2008]. This is part of Von Karman vortex streets [*Hernández-Guerra et al.*, 1993; *Pacheco and Hernandez-Guerra*, 1999], which is conducive to the "Canary Corridor" of long-lived mesoscale ocean eddies [*Sangrà et al.*, 2009]. The wind pattern at the eastern boundary is also characterized by an equatorward wind jet that flows near the African shelf [*Bakun and Nelson*, 1991; *Mittelstaedt*, 1991].

The RAPID measurements have shown a large seasonal cycle in the AMOC of over 6 Sv. The largest contribution to this seasonality arises from the basin-wide geostrophic flow across the basin between the Bahamas and the Canary Islands [*Kanzow et al.*, 2010; *Chidichimo et al.*, 2010]. Seasonal variations in wind stress curl near the eastern boundary is the forcing mechanism attributed by *Kanzow et al.* [2010] to the seasonal variations in the AMOC transports. They forced a simple Rossby wave model with wind stress curl to recover the

phase of the seasonal cycle of the AMOC transports. Westward traveling Rossby waves in the Canary basin have been discussed by a number of authors [*Siedler and Finke*, 1993; *Osychny and Cornillon*, 2004; *Hirschi et al.*, 2007; *Sangrà et al.*, 2009; *Mason et al.*, 2011]. The presence of Rossby waves in the lee region of oceanic islands has also been observed in the Hawaiian archipelago where they are considered a direct consequence of the mesoscale activity and the wind stress curl [*Xie et al.*, 2001; *Belmadani et al.*, 2012; *Lumpkin and Flament*, 2013]. A careful analysis of the empirical orthogonal functions (EOFs) associated with the wind by *Duchez et al.* [2013] shows that the density fluctuations south of the islands are driven by the wind stress curl and directly influence the AMOC. Equatorward wind stress and cyclonic wind stress curl characterizes the region nearest the African shelf. In *Longworth et al.* [2011], it is suggested that the weak upwelling scenario in spring/winter, decreases the basin-wide thermocline slope and leads to a weaker southward transport of the mid-ocean, while the opposite occurs in summer/fall, when the upwelling intensifies (see their Figure 4).

This paper explores the contribution of the Canary Basin dynamical processes to the seasonal behavior of the AMOC. To fulfill this objective the RAPID array data will be compared with a mooring deployed at the LP. These different hydrographic data will be used together with wind and altimeter data and with a Rossby wave model in order to achieve a good knowledge of the geographical study area. The study is divided into the following sections: starting with (2) an exposition of data and (3) methods used, followed by (4) a detailed results section, and finishes with (5) an extensive discussion of the results.

2. Data

This study compares moored hydrographic data from two different moorings, the Eastern Boundary Current 4 (EBC4) mooring and a merged product from the RAPID array referred to as EBH (Figure 1).

During the CANIGO project, several current meters were installed in four moorings deployed in the LP between January 1997 and January 1999 (the EBCs) [*Knoll et al.*, 2002]. At the end of this project, it was decided to maintain one of the four moorings, the EBC4, as it was representative of the circulation through the passage [*Hernández-Guerra et al.*, 2003]. The EBC4 has been collecting data since January 1997. For this study we will use the velocity (transport) time series until December 2012 (February 2006). Current meters were located at representative depths of 150, 300 and 500 m for NACW, 870 for AAIW and 1230 m for MW. The newest mooring design installed as of March 2008, includes a high resolution Acoustic Doppler Current Profiler (ADCP) that improves the velocity measurement from 150 m to the sea surface.

The RAPID array, is a basin-wide dynamic height array that consists of several moorings at 26°N, equipped with conductivity-temperature-depth (CTD) sensors. These moorings are located on the western boundary, on both flank of the mid-Atlantic ridge and a series of moorings along the eastern boundary (Figure 1). The RAPID time series that is used in this paper expands over a decade (2004–2014). The AMOC, calculated from the RAPID array, is estimated by combining the RAPID array with ERA-Interim winds [*Dee et al.*, 2011] and the transport from cable measurements in the Straits of Florida [*Meinen et al.*, 2010].

The wind product that was chosen to study the seasonal variability of the wind stress curl around the Canary Basin is the Scatterometer Climatology of Ocean Winds (SCOW). This climatology covers 122 months from September 1999 to October 2009 of QuikSCAT scatterometer data (SCOW, http://numbat.coas.oregonstate.edu/scow/). The SCOW climatology has a resolution of 1/4 of a degree and resolves the effect that islands have on the path of the atmospheric flow [*Risien and Chelton*, 2008]. SCOW is also used together with the *Levitus* [1982] Climatology to repeat the experiment carried out in *Kanzow et al.* [2010]. This study updates the observations of the seasonal cycle of the AMOC to 2014, more than doubling the time period of analysis of *Kanzow et al.* [2010].

Some additional data were used to carry out this work. Mapped Absolute Dynamic Topography (MADT) and Mapped Sea Level Anomalies (MSLA) were downloaded from AVISO from October 1992 to December 2012 (http://www.aviso.oceanobs.com/, downloaded the 27 November 2013).

3. Methods

The AMOC strength, calculated from the RAPID array, is defined as the maximum of the overturning stream-function resulting from the sum of transport-per-unit-depth data from three components: wind-driven Ekman transport, Gulf Stream (GS) transport and mid-ocean transport from moored instruments stretching

from the Bahamas to the Canary Islands (Figure 1). The geostrophic transport per unit depth between the eastern and western boundaries can then be expressed as:

$$T_{geo}(z,t) = \int_w^e (v_{dh}(x,z,t) - v_r(t))dx = \frac{1}{f}(\Phi_e(z,t) - \Phi_w(z,t)) + v_r w(z), \qquad (1)$$

where f stands for the Coriolis parameter and $w(z)$ for the width of the basin at each depth level. The dynamic height (Φ) is calculated at the eastern and western boundaries referenced to 4820 dbar (e and w subscripts, respectively); hence, the velocity is the result of adding a contribution derived from the dynamic heights (v_{dh}) and a contribution arising from a constant velocity at the reference level (v_r). Therefore, in this paper, we will neglect the dynamic height contribution from the mid-Atlantic ridge moorings.

The reference level velocity is estimated by adding the components of the flow and solving for v_r such that the overall flow across the section at each time step is zero.

$$T_{fs}(z) + T_{wbw}(z) + T_{ek}(z) + \frac{1}{f}(\Phi_e(z) - \Phi_w(z)) + v_r w(z) = 0, \qquad (2)$$

where the subscripts fs and ek refer to the depth-distributed Florida Straits transport and the wind-driven Ekman transport. The western boundary wedge (wbw) is different from the western boundary dynamic height ($\Phi_w(z)$). The western boundary wedge is estimated from direct current meter measurements west of the WB2 mooring while the western boundary is estimated from the dynamic height measured at the WB2 mooring (Figure 1b). On the other side of the basin, the eastern boundary is estimated from the dynamic height measurements ($\Phi_e(z)$) of the moorings east of the EBH1 (Figure 1c).

The different flow contributions of equation (2) are integrated vertically from the bottom to the surface to provide with a vertical stream function. The maximum value of this stream function is the strength of the AMOC:

$$AMOC = max\left(\int^z T_{fs}(z) + T_{wbw}(z) + T_{ek}(z) + T_{geo}(z)\right)dz \qquad (3)$$

The integration in equation (3) also provides the depth of the maximum value of the vertical stream function, which turns out to be about 1100 m. Hence, we may use this depth (z_{AMOC}) to define the upper mid-ocean flow (UMO) as follows:

$$UMO = \int_0^{z_{AMOC}}(T_{wbw}(z) + T_{geo}(z))dz, \qquad (4)$$

The UMO flow is usually thought of as the southward gyre circulation. The circulation at the RAPID array latitude (26°N) can then be described by:

$$AMOC \approx UMO + GS + Ekman \approx -NADW. \qquad (5)$$

where GS refers to the Gulf Stream in the Florida Straits. This holds true when the depth of the overturning is deeper than the depth of the Florida Straits, as is generally the case. Hence the transport of the AMOC equals the deep southward transport of mainly North Atlantic Deep Water (NADW) with a minor contribution from Antarctic Bottom Water. This formula neglects the northward flow of Antarctic Bottom Water but is a useful way to consider the circulation. Full details of this calculation can be found in *McCarthy et al.* [2015].

The upper level of RAPID moorings is targeted to 50 m. Moorings whose top buoy is on the surface suffer higher loss rates due to greater vulnerability with extreme weather and fishing activity [*McPhaden et al.*, 2010]. Frequently the depth of the shallowest instrument is deeper
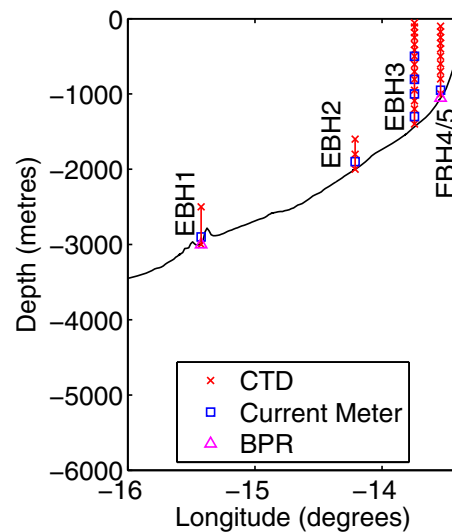
Figure 2. Individual moorings that are merged to cover the water column from surface to 5000 m, referred to as the EBH array. The top 1000 m is covered by mooring EBH4/5, 1000–1500 m is by EBH3, 1500–2000 m by EBH2, 2000–2500 m by EBH1. Deeper moorings are not discussed in this text. Microcat (CTD) data are illustrated with red crosses, current meters with blue squares and bottom pressure measurements with magenta triangles.
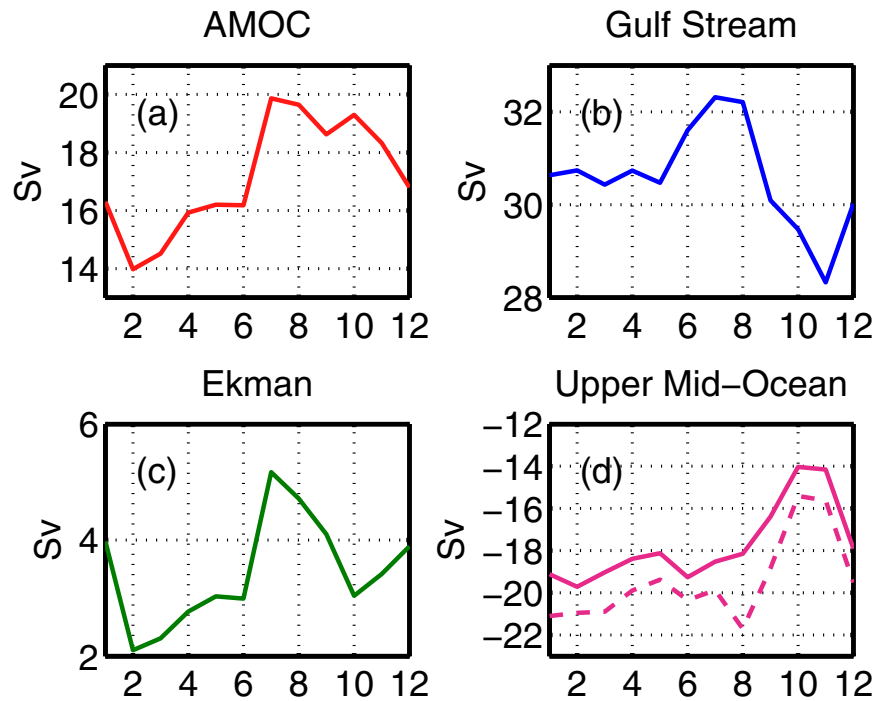
Figure 3. Seasonal cycles of the components of the (a) AMOC: (b) the Gulf Stream, (c) Ekman Transport, and (d) the Upper Mid-Ocean: upper mid-ocean transports (solid magenta line), upper mid-ocean minus western boundary wedge (dashed magenta line). Note different y axis ranges for each plot. x axis represents the months of the years.
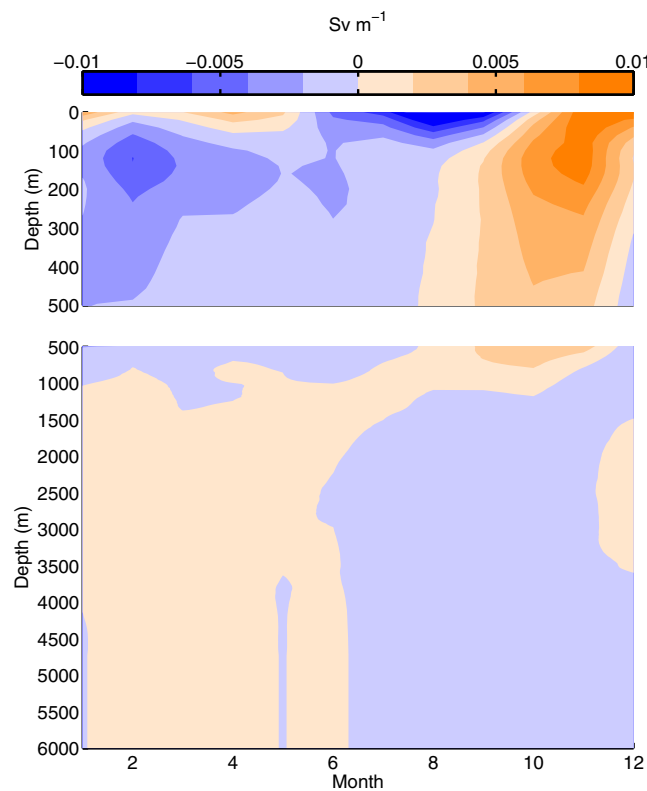
Figure 4. Seasonal anomalies of the mid-ocean transport per unit of depth derived from dynamic height difference between the eastern and western basins (Sv m^{-1}).

than 50 m. Because of this, the dynamic height is extrapolated from the shallowest instrument to the surface using a seasonal climatology [*McCarthy et al.*, 2015]. This allows us to examine the seasonal cycle in the uppermost layers for the first time.

The individual moored CTD measurements from the EBH moorings are merged and gridded as described in *McCarthy et al.* [2015], resulting in a single 20 dbar gridded profile at the eastern boundary for each time step. The result is a single temperature and salinity profile representing the full eastern boundary from the surface to 5000 m. The vertical distribution of the instruments in the EBH array is shown in Figure 2.

4. Results

4.1. The Circulation at 26°N

Figure 3 shows the seasonal average of the components of the
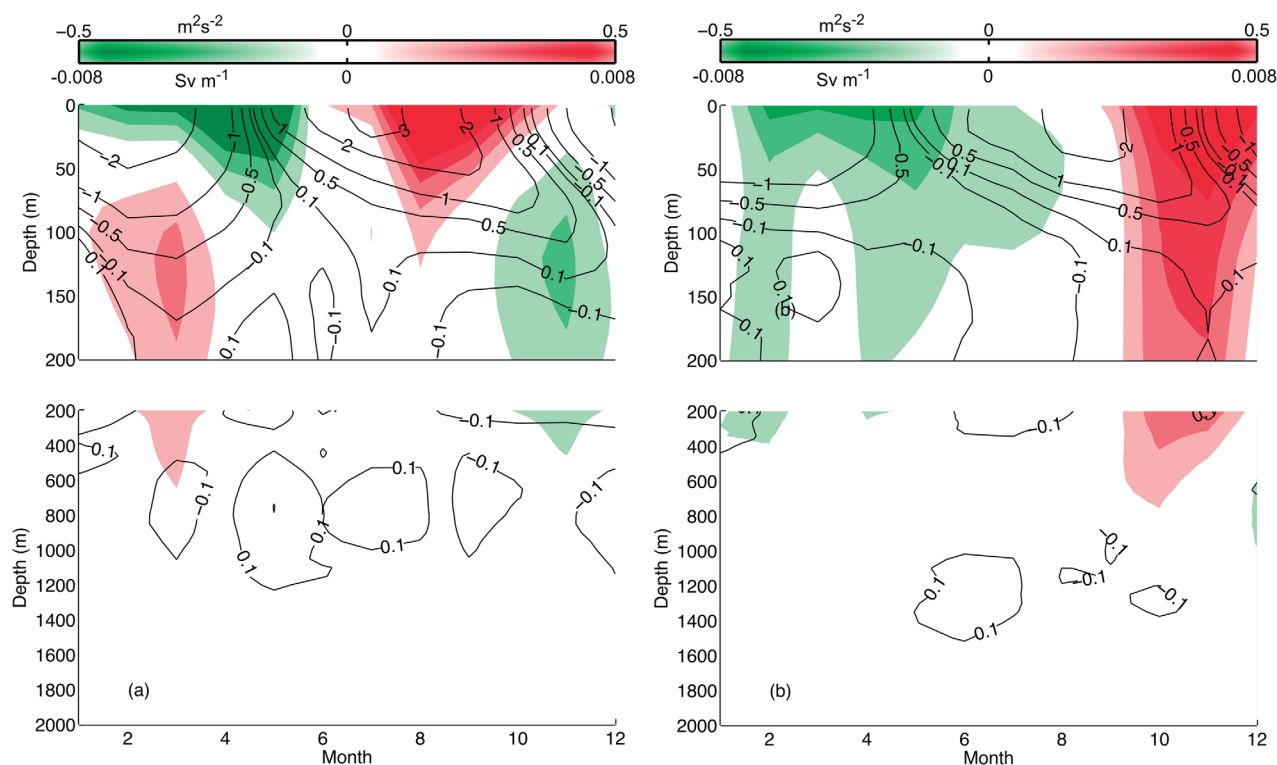
Figure 5. Seasonal anomaly relative to the mean dynamic height profile (calculated from 2004 to 2014) on the (a) western boundary and (b) eastern boundary with the mean annual profile removed. Seasonal temperature anomalies (°C) from Argo climatology are overlaid in black contours. Scaling of the dynamic height anomalies to transport per unit depth anomalies is provided by dividing by the Coriolis parameter to allow comparison with Figure 4.

basin-wide transport as measured by the RAPID array. The seasonal cycle has a peak to trough value of over 6 Sv. The AMOC peaks at 3 different months; February, July, and October. The AMOC shows a minimum peak in February when the UMO is strongest southward and the Ekman transport is weakest northward. In July, a maximum peak in the AMOC occurs when the Gulf Stream and Ekman transports are at their maximum transport. The second maximum peak of the AMOC occurs in October and coincides with the weakest southward flow in the UMO. The seasonal cycles of Ekman transport and the Florida Straits transport have been the focus of previous studies [*Meinen et al.*, 2010; *Atkinson et al.*, 2010] and will not be discussed further here.

The UMO is the largest single contributor to the seasonal cycle of the AMOC. The direct current meter measurements in the western boundary wedge do not contribute significantly to the seasonal cycle of the UMO (Figure 3d). Therefore we can discuss the seasonal cycle of the UMO in terms of the dynamic height difference between the eastern and western boundaries (T_{geo} in equation (4)). The seasonal cycle of the full mid-ocean transport-per-unit-depth is shown in Figure 4. The major feature in the seasonal transport is the anomalously positive transports above 1000 m depth from August to December that peak in October. This shows that the depth structure of the seasonal cycle of the mid-ocean transports is driven by variability in the top 1000 m, which is essentially the UMO transport. In February, at near 100 m depth, there is an anomalously southward transport. This negative anomaly is smaller than the positve anomaly in October, giving the seasonality of the UMO transport an assymetry. In the most shallow layers, at depths less than 50 m, there is a seasonal cycle driven by differences in seasonal warming at the eastern and western boundaries.

Below 1000 m there is weak anomalously positive flow from January to July. This flow reverses from July to December. This reversal near 1000 m and the fact that the deep flow acts in the opposite direction to the flow shallower than 1000 m gives the seasonal anomalies a signature of first baroclinic mode variations [*Clément et al.*, 2014]. The variations deeper than 1000 m are weakly baroclinic. Baroclinic variations in the water masses deeper than 1000 m are important for understanding interannual variability [*McCarthy et al.*,
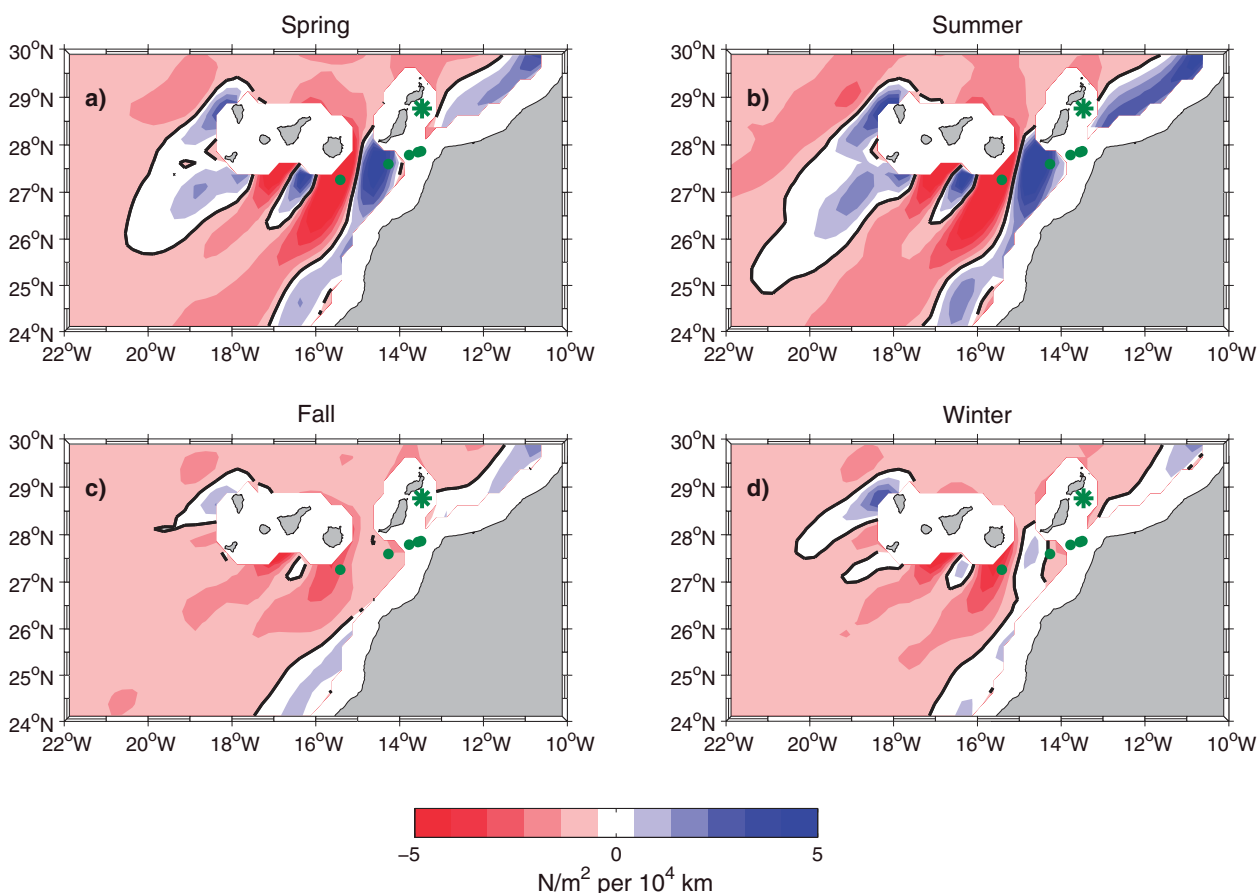
Figure 6. Mean wind stress curl around the Canary Islands per season from the SCOW climatology. The zero wind stress curl is highlighted with a thick black line. Green dots and asterisks represent the location of the EBH array and EBC4 moorings, respectively.

2012] but on seasonal timescales this flow reflects the barotropic compensation of Ekman, Florida Straits and UMO transport across the basin.

To further understand the seasonal cycle of the mid-ocean, we examine the dynamic height on the east and west ends of the basin. In the upper 50 m, the thermal structure is influenced both by the seasonal cycle of sensible heat fluxes and latent heat fluxes, the latter driven primarily by the wind. The wind can also affect the thermal structure of the upper ocean by changing Ekman and Sverdrup transport. At 26°N, thermal anomalies in the upper ocean are far more important than haline anomalies for density and, consequently, dynamic height changes. If these temperature changes occur evenly across the basin, then no geostrophic transport emerges. Figure 5 shows that the temperature changes do not occur evenly across the basin. The coolest temperatures on both sides of the basin occur in February. However, warmest temperatures in the west occur in July, and in August/September on the eastern boundary. This lagged warming response in the east leads to the strong southward transport in the top 100 m in August as seen in Figure 4.

Below the top 50 m, the western boundary shows a reversing positive to negative pattern around 120 m depth (Figure 5). This is maximum in February/March and minimum in November. This contributes to the anomalously southward (northward) flow in the UMO in February (November). Figure 5 shows that the major source of seasonal variability in the UMO and, consequently, the AMOC is due to the eastern boundary in fall. While the contribution to the seasonal cycle of the UMO due to the west in fall is overwhelmed by the variability on the eastern boundary, the western boundary dynamic height is the major contribution to the minimum of the UMO in February as there is no corresponding eastern boundary signal.

Beginning in August and persisting until December, a positive dynamic height anomaly develops that stretches from 1000 m to the surface (Figure 5). This feature was identified previously by *Kanzow et al.*
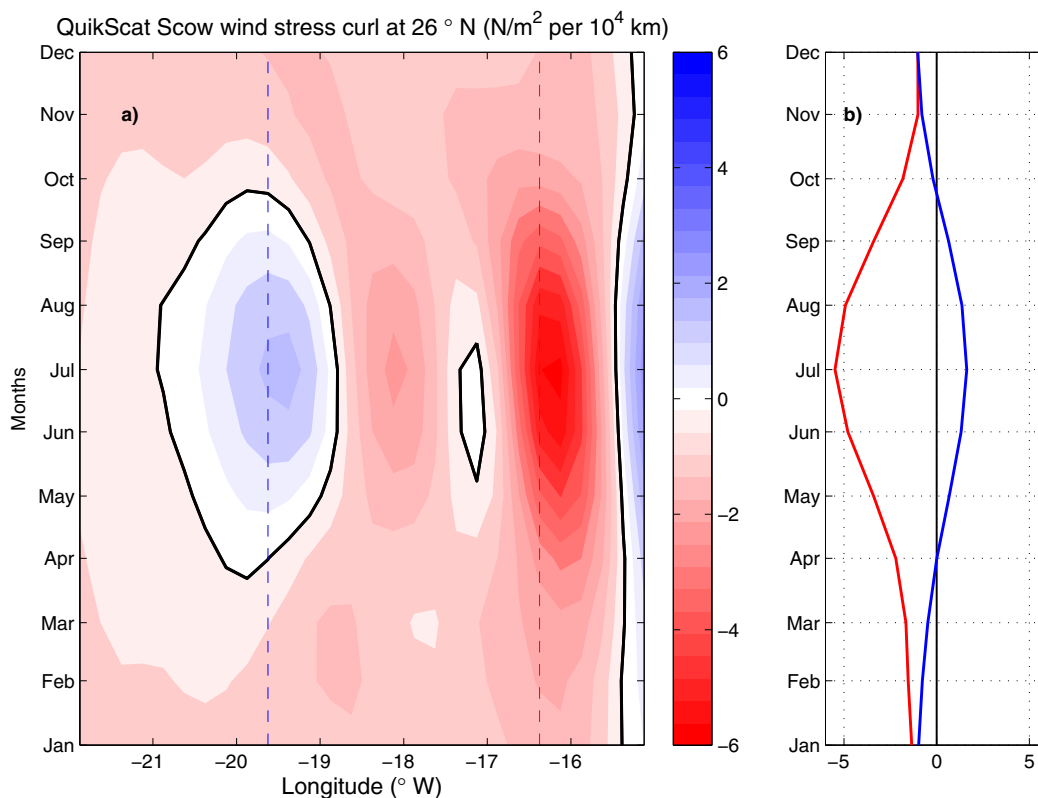
Figure 7. (a) Seasonal wind stress curl anomaly at 26.12°N using the SCOW climatology. The zero of the wind stress curl is highlighted with a black contour. Dashed lines are placed indicate the locations of wind stress curl used in Figure 7b. (b) Wind stress curl at 19.62°W (blue) and 16.37°W (red).

[2010] and *Chidichimo et al.* [2010] as the main contributor to the seasonal cycle of the AMOC at 26°N. A simple Rossby wave model was used to link this anomalously northward transport in fall to the wind stress curl forcing at the eastern boundary.
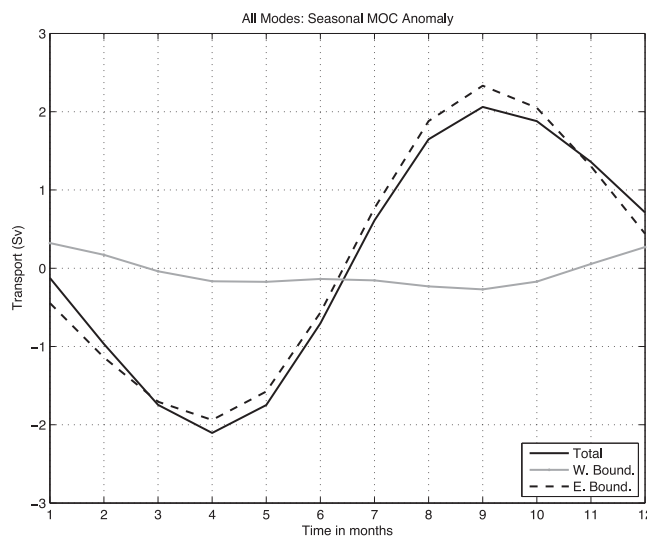

Figure 8. The mid-ocean transport anomaly derived from the forced Rossby wave model summed over the first two baroclinic modes (solid black line). The eastern (dashed black line) and western (grey solid line) contributions to the total transport anomaly are highlighted.

The remainder of this paper will focus on explaining this eastern boundary transport anomaly in the context of the regional circulation around the Canary Islands.

4.2. Seasonal Cycle of Winds Around the Canary Islands

Figure 6 reveals the cyclonic and anticyclonic structures that emerge from the interference of the islands on the mean southward wind circulation. These structures can be observed during all four seasons, being stronger in spring and summer and weaker in fall and winter according to the wind stress curl (Figures 6 and 7). In addition, Figure 6 shows a wide continuous cyclonic wind stress curl along the coast, extending as far as this zero line.
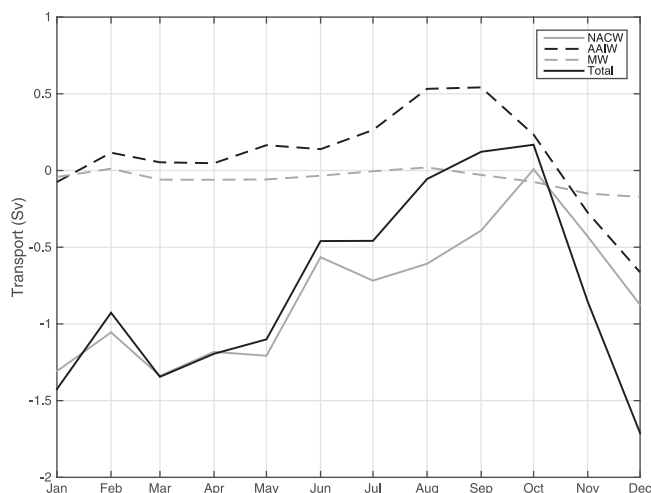
Figure 9. Seasonal transport of the EBC4 mooring in the LP (solid black line) and each of the water masses that flow through it: NACW (solid grey line), AAIW (dashed black line) and MW (dashed grey line).

The zero wind strength curl line relies where the wind stress has its maximum strength.

As observed in Figure 6, the zero of the wind stress curl line moves seasonally. In fall and winter, when the wind stress curl is the weakest, the zero curl line is the closest to the African shelf. During summer this line moves offshore, almost along the line of Fuerteventura and Lanzarote Islands (Fuerteventura can be translated as strong winds). The easternmost EBH moorings lie inside the along shore cyclonic wind stress curl. In contrast, the EBC4 is located in positive and negative wind stress curl regimes depending on the season (Figure 6).

Figure 7a shows the seasonal pattern of wind stress curl at 26°N, in the lee of the islands, where the RAPID array is located. The tallest islands of the archipelago are Tenerife (3718 m), La Palma (2426 m) and Gran Canaria (1949 m) while the shortest islands are those to the east. July is the month with the strongest wind stress curl and therefore is the month where the greatest seasonal change is observed (Figure 7a). The large anti-cyclonic structure is generated downstream of Gran Canaria, while the cyclonic structure it is due to the westernmost islands.

Figure 7b shows the evolution of the two wind stress curl positive and negative structures located at 19.62°W and 16.37°W, respectively. The figure reveals that their absolute maximum is achieved during July with different signs, while their minima (negative values) occur during fall and winter. The wind stress curl also induces vertical velocities through Ekman pumping. *Piedeleu et al*. [2009] observed that the wind stress curl may act as an additional eddy-generation trigger mechanism when the impinging oceanic flow is not sufficiently intense, therefore, inducing changes in the density field. The observed strong alternating negative to positive wind stress curl structures at a distance of 220 km south of the islands, induce positive/negative Ekman pumping that will generate Rossby waves.

4.3. Rossby Wave Response to Wind Forcing

In *Sturges and Hong* [1994], a simple model is used to study the low-frequency large-scale wind-driven response of the ocean. This model provides an estimation of the long Rossby wave speed as a function of longitude. *Kanzow et al*. [2010] modified the model in order to observe the eastern and western boundary contributions to the overall cross section wind-stress response at the latitude of 26.5°N. The response of the seasonal eastern boundary is the local forced solution of the eastern boundary, while the western boundary shows the locally forced solution at the western boundary plus the accumulated effects of Rossby wave propagation from forcing west of the mid-Atlantic ridge.

In this section, the experiment in *Kanzow et al*. [2010] is repeated using the SCOW winds and the Levitus climatology [*Levitus*, 1982] to obtain the representative vertical modes. The linear, subinertial response of a stratified ocean to wind stress curl variability can be expressed in terms of vertical modes that arise from applying an Empirical Orthogonal Analysis to the density anomaly field across the section. Equations and further explanation can be found in *Kanzow et al*. [2010]. As mentioned in section 4.2, the wind stress curl has a semiannual signature in the Canary basin. This wind stress curl behavior induces changes in the eastern boundary isopycnals and leads to the formation of Rossby waves. We force the model using winds near 16°W, which is in the middle of the anti-cyclonic structure on the eastern lee side of the islands. This location is quite different to that chosen by *Kanzow et al*. [2010], but it highlights the effect that the wind stress curl has on the Rossby waves.

Figure 8 is analogous to the Figure 14a of *Kanzow et al*. [2010], where the first two baroclinic modes are summed. The model shows that the UMO transport is very sensitive to seasonal transport changes at the
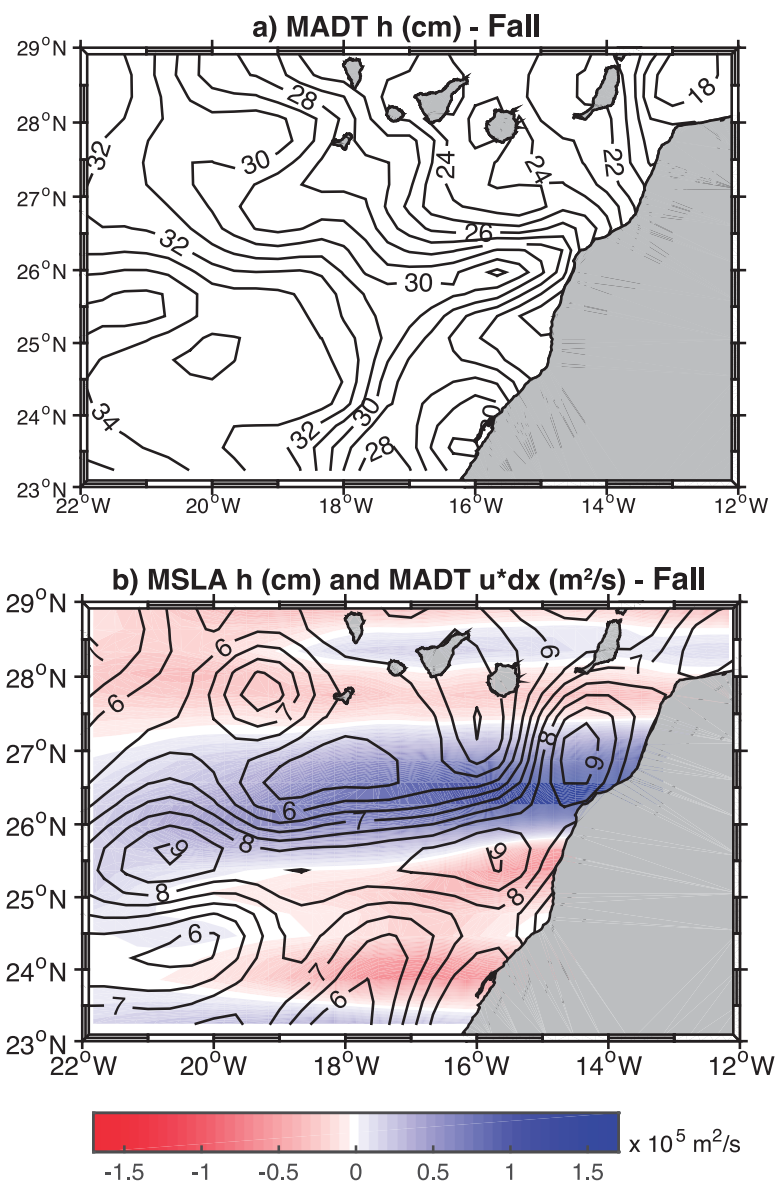
Figure 10. (a) AVISO Mapped Absolute Dynamic Topography (MADT) dynamic height (black contours, centimeters) and (b) west to east zonal accumulation (starting at 24.5°W) of the zonal integrated velocities (colored, squared meters per second) together with the Mapped Sea Level Anomalies (MSLA) (black contours, centimeters) in the fall season.

eastern boundary, as their predicted values are nearly coincident (Figure 8). This result implicates that the wind stress curl south of the Canary archipelago changes the stratification at the eastern boundary. These changes are key for the formation of Rossby waves and directly affect the seasonal cycle of the UMO. Figure 8 also reveals a 3 month lag between the maximum wind stress curl in July (Figure 7) and the maximum of the Rossby wave driven transport in September (Figure 8).

The Rossby wave model successfully explains much of the seasonal cycle that is observed, including the 3 month lag between the maximum of the wind forcing and the maximum transport. In contrast, there are several questions that remain. First, Figure 8 has a good correspondence with the seasonal cycle of the UMO shown in *Kanzow et al.* [2010] Figure 10, but the correspondence with our seasonal UMO is not as good (Figure 3). Their average seasonal UMO has been estimated in between 2004 and 2008, while the seasonal UMO shown here, in Figure 3, was estimated in between 2004 and 2014. Second, even though they both peak in October the observed seasonal cycle of UMO is not symmetric, with the peak in October being larger than the trough in February (e.g., Figure 3). Third, *Kanzow et al.* [2010] computed the model using
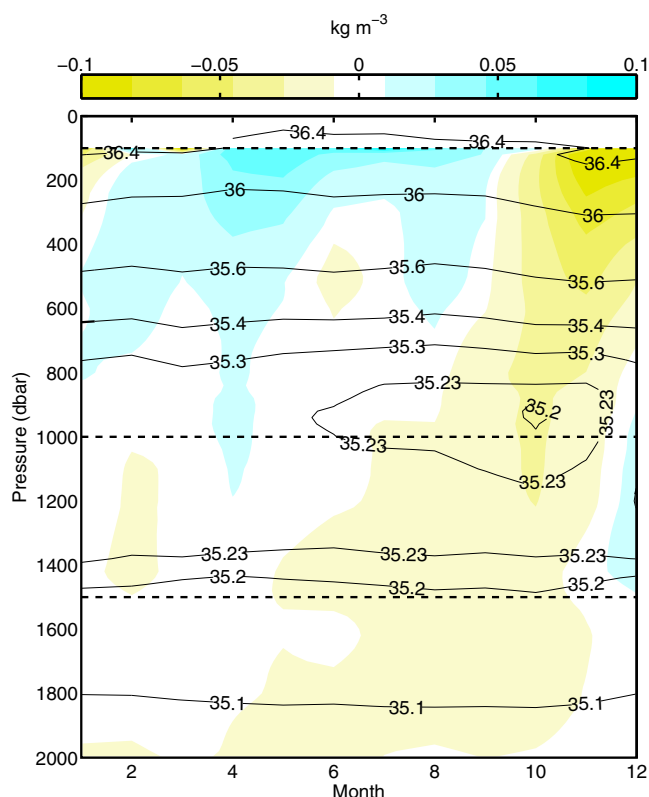
Figure 11. EBH seasonal density anomaly (colored contours) together with the seasonally averaged salinity (black contour) derived from Argo data. Horizontal dashed lines indicate breaks between individual moorings that constitute EBH.

winds along the whole 26.5°N, while this study choses to use wind stress curl in the lee of the island. Comparing the results shown in Figure 8 with *Kanzow et al.* [2010] (Figure 14a), the main difference between both figures is a month lag, but the amplitude and the conclusions coincide. This suggests that the different wind western extensions did not significantly affect the results, being the area south of the Canary islands the main driver of the seasonal transports. Fourth, this model shows a seasonal peak to peak amplitude of 3 Sv, while the UMO has a peak to peak seasonal amplitude of 4 Sv.

4.4. The Lanzarote Passage
4.4.1. The Recirculation of the Canary Current

The LP transport, as revealed by the EBC4 mooring, has a positive peak in October that coincides with the weakest southward transport of the UMO (Figure 9). This figure also suggests that the highest contribution to the total transport is made by the NACW in the thermocline layers.

Unique to the fall season, a zonal structure in dynamic height is formed south of the islands around 26.5°N (Figure 10). As reported in *Machín et al.* [2006], *Laiz et al.* [2012], and *Pérez-Hernández et al.* [2013], in Figure
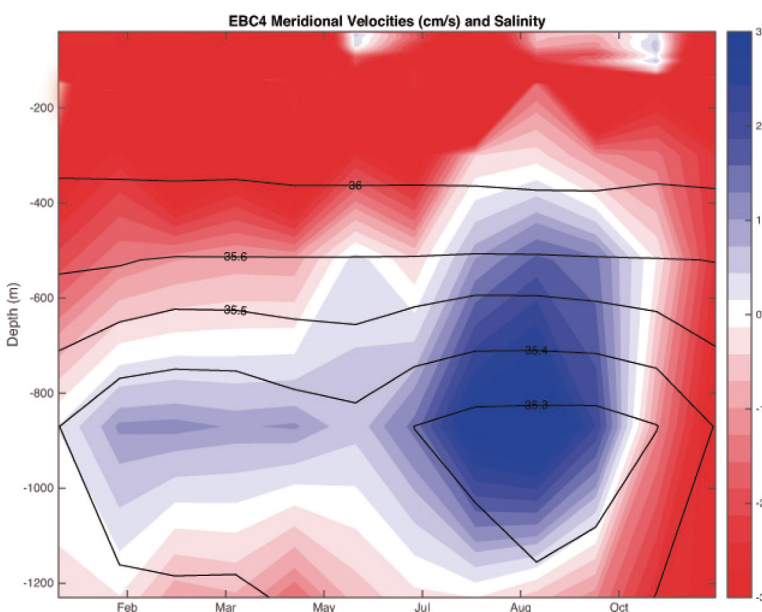
Figure 12. EBC4 seasonal meridional velocities (color contours) together with salinity (black contours).
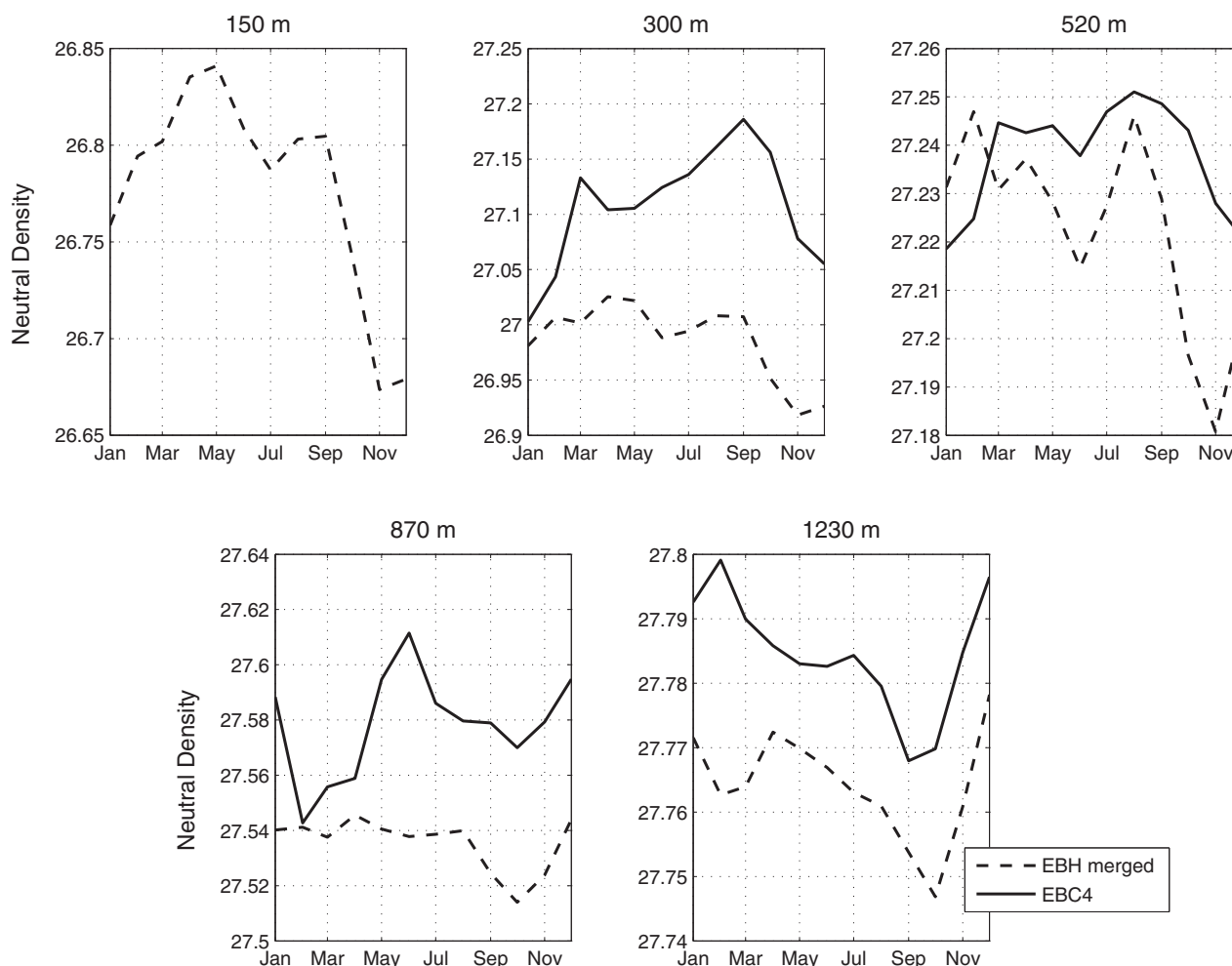
Figure 13. Densities at selected depths at the EBH array (dashed line) and EBC (solid line).

10a the CC in fall is located at its westernmost position, west of the island of La Palma. This same figure shows a partial zonal bifurcation of the flow around 26.5°N. Figure 10b, shows that the zonal bifurcation is characterized by eastward velocities (blue) and that once it reaches the African shelf the MSLA (black contour) diverts northward into the LP. The eastward flow that is formed in the lee of the Canary Islands during fall is the driving mechanism of the surface recirculation of the CC through the LP observed in fall (Figure 10).

4.4.2. The Intermediate Poleward Undercurrent (IPUC)

The IPUC flows seasonally northward through the LP (Figure 9). When the IPUC is strongest to the north, the proportion of AAIW in the region increases [*Hernández-Guerra et al.*, 2003; *Machín and Pelegrí*, 2009; *Pérez-Hernández et al.*, 2013] and this causes lower salinities as observed at EBH in Figure 11 and at EBC4 in Figure 12. In Figure 13, the density at the five EBC4 depths shows an stretching of the isoneutrals between the 300 m and 1230 m depth. The stretching is more evident in the EBC4 than in the EBH array eastern boundary moorings. This is probably due to the high mesoscale activity that can be found south of the Canary Islands [*Aristegui et al.*, 1994; *Sangrà et al.*, 2009]. Density at 1230 m decreases to a minimum in September whereas density at 300 m increases to a maximum in September, consistent with a layer stretching in between. Most other depths (520 m and 890 m) show an evolution similar to the 300 m depth, highlighting that it is the intermediate layer near 1000 m that stretches, a view consistent with the salinity evolution of Figures 11 and 12.
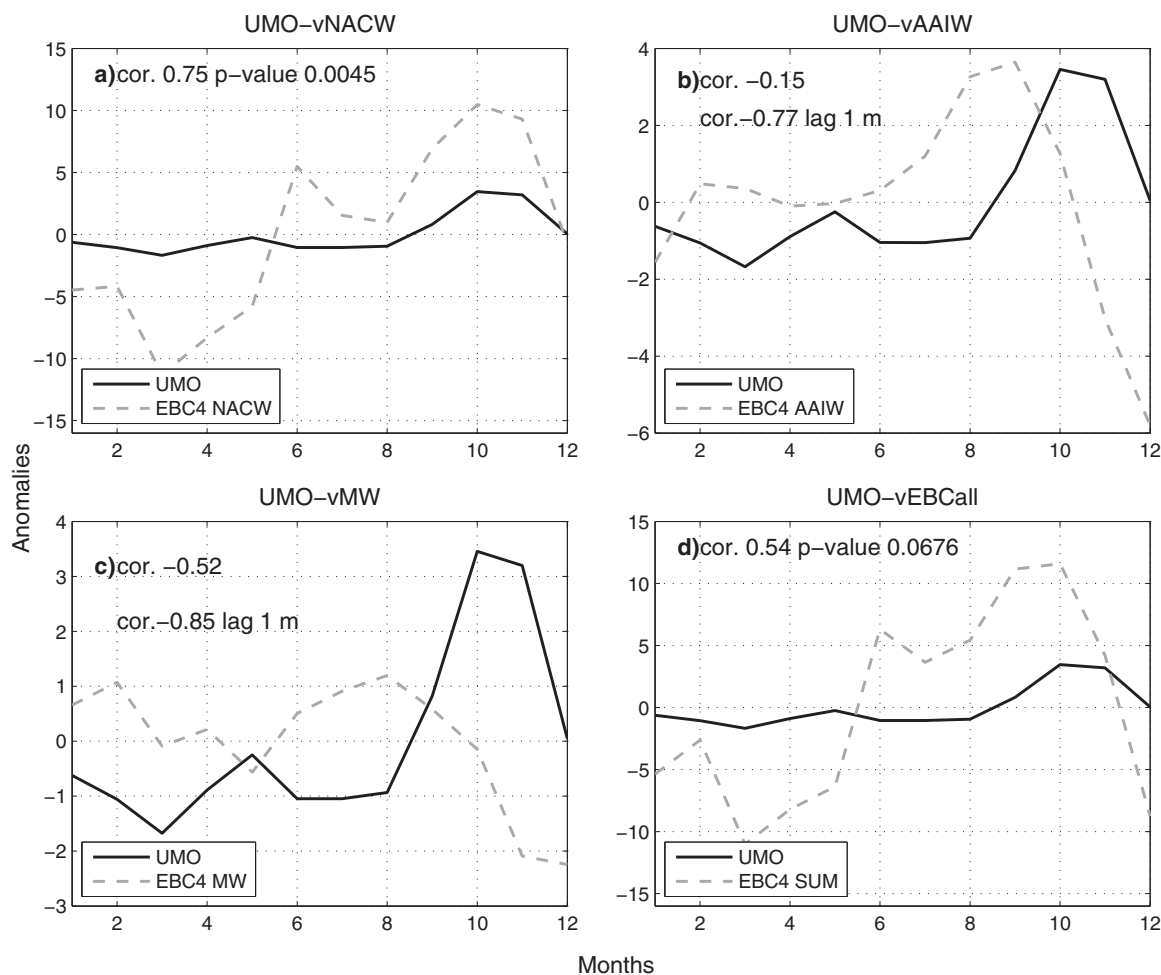
Figure 14. Seasonal anomalies (minus the annual mean) curves of the UMO transport (black solid lines) and the rotated meridional velocity of each component of the EBC4 (dashed grey lines): (a) NACW, (b) AAIW, (c) MW, and the (d) total. Significant correlations are shown.

4.5. The Lanzarote Passage and the Upper Mid-Ocean Seasonal Behavior

The seasonal density changes of the EBH array are shown in Figure 11. Dynamic height is an integral form of the density structure where negative density anomalies contribute to positive dynamic height anomalies and, unless balanced elsewhere, result in northward flow. The peak of the maximum northward seasonal anomaly in the UMO transports occurs in October-November at roughly 200 m (Figure 4). The surface maximum northward anomaly matches with the behavior of the NACW of the LP. The NACW of the LP reaches its minimum southward transport during fall, and in some years it even reverses northward during November [*Hernández-Guerra et al.*, 2003; *Fraile-Nuez et al.*, 2010]. Figure 14a shows that during fall, both the velocity of NACW at the LP and the transport of the UMO reach their weakest southward intensity. In Figure 9, it is observed that the velocity of the NACW at the LP even reverses in October. A significant correlation of 0.75 is found between the anomalies of the meridional velocities of the LP NACW and the anomalies of the UMO transport (Figure 14a).

While the peak in the maximum northward anomaly in the UMO transport occurs in October-November at roughly 200 m, it is observed that the low density anomalies emerge in July at 900 m approximately, where a salinity minimum can be found (Figure 11). This also relates the UMO with the LP. In Figure 12 a northward velocity core appears at roughly 800 m from July to October together with low salinities. This core seems to spread to almost all the LP in September, decreasing the surface southward flow to velocities lower than −1.5 cm/s in October.

UMO transport and the transport of the northward/southward AAIW/MW flow recorded in the LP, presents a high correlation (0.77/0.85) at 1 month lag (Figures 14b and 14c). This indicates that the RAPID moorings

observe the signal a month before the EBC4, implying velocities of approximately 2.6 cm/s. This lagged correlation also shows that the intermediate layers do not reverse at the same time as the upper layers, suggesting different driving mechanisms.

5. Discussion and Conclusions

This study has described in detail the basinwide geostrophic transport derived from dynamic height differences between eastern and western boundaries that constitute the largest component of the seasonal cycle of the AMOC at 26°N and also has described the eastern boundary contribution to this transport in terms of the local circulation around the Canary Islands. The AMOC has a seasonal peak to trough value of 6 Sv, with two maxima in July and October. The October peak coincides with the weakest southward transport of the UMO. The seasonally averaged dynamic height shows that the major source of seasonal variability in the UMO is due to the eastern boundary in fall. The eastern boundary is the dominant source of seasonal variability, as has been established previously in observations [*Kanzow et al.*, 2010; *Chidichimo et al.*, 2010], high resolution ocean models [*Mielke et al.*, 2013; *Duchez et al.*, 2013] and simplified models [*Zhao and Johns*, 2014; *Yang*, 2015].

The winds in the Canary Basin show a high seasonality in strength. SCOW wind stress curl showed the presence of the Von Karman streets south of the islands and the continuous cyclonic wind stress domain near the African shelf, as in *Bakun and Nelson* [1991], *Desbiolles et al.* [2014], and *Mason et al.* [2011]. The wind stress curl generates a strong seasonal structure at a distance of approx. 200 km south of the islands that will induce Rossby waves. This is has also been observed in other islands such as the Hawaiian archipelago [*Xie et al.*, 2001].

A Rossby wave response to the seasonal cycle of wind stress curl at the eastern boundary was proposed as a mechanism of the seasonal variability [*Kanzow et al.*, 2010]. The Rossby wave transport response successfully recreated the approximately 3 month lag between the maximum wind forcing and the maximum transport response. However, its seasonal transport does not resemble that of the observed UMO. In addition, it is heavily influenced by the local wind patterns induced by the presence of the tall Canary Islands close to the African coast. This begs the question of whether it is a sufficient mechanism to explain the large meridional coherence of the seasonal cycle through out the subtropical North Atlantic [*Mielke et al.*, 2013; *Zhao and Johns*, 2014]. In addition, the Rossby wave transport does not capture the apparent remote forcing such as subpolar wind stress curl that is seen to influence the seasonal cycle at 26°N [*Yang*, 2015].

A relationship between the circulation in the LP and the AMOC, was first suggested in *Fraile-Nuez et al.* [2010] and *Chidichimo et al.* [2010]. Significant correlations can be found between the LP transport and the UMO, where the NACW from the EBC4 is correlated 0.75 at zero lag, and the transport of AAIW/MW at the same mooring are correlated 0.77/0.85 respectively, with a lag of 1 month with the UMO. The month lag indicates that the intermediate reversal found in the LP is detected at 26°N ahead of EBC4, while the surface reversal occurs at the same time in both moorings. This suggests two separate driving mechanisms for the northward surface and intermediate flow observed in fall at the LP.

Estimations from altimetry done on the lee region of the islands (Figure 10), support that part of the CC recirculates eastward throughout the lee region during fall and diverts the CC northward into the LP. The model of *Mason et al.* [2011] showed a similar recirculation pattern south of the archipelago, in their Figure 7. South of 25.5°N westward velocities are observed accompanied by two anticyclonic eddies (Figure 10b).

Sangrà et al. [2009] defined the Canary Eddy Corridor between 22°N and 29°N. They described that at around 25°N and 18°W, eddies sense a β-effect that forces them to propagate westward, forming the Canary Corridor. This westward corridor presents a dominance of anticyclonic over cyclonic eddies. This kind of long-lived eddy corridor also exists in other oceanic regions such as the Hawaiian Islands [*Calil et al.*, 2008].

The observed pattern of eastward velocities over westward velocities observed between 24°N and 27°N in Figure 10b, is similar to the one described in Hawaii. In Hawaii, the eastward Hawaii Lee Countercurrent is believed to be fed by the anticyclonic eddies that are shed from Big Island of Hawaii and that are propagating westward, immediately south of the Hawaii Lee Countercurrent [*Xie et al.*, 2001; *Lumpkin and Flament*, 2013]. In Figure 10b, we can observe a clear area of eastward velocity and immediately beneath it, around

25.5°N, westward velocities are seen together with two anticyclonic eddies. The latitude of these westward velocities that appear with anticyclonic eddies matches the description given in *Sangrà et al.* [2009] for the Canary Corridor. In addition, this kind of structure where eastward velocities are found over westward velocities, resembles the pattern described for the Hawaiian archipelago in *Xie et al.* [2001] and *Lumpkin and Flament* [2013]. Therefore, it is possible that the Canary Corridor could be reinforcing the formation of an eastward recirculation of the CC south of the archipelago in fall, as occurs in the Hawaiian archipelago.

In contrast, the IPUC at the LP is attributed to the stretching of the isopycnal caused by the remote forcing explained in *Machín and Pelegrí* [2009]. *Fraile-Nuez et al.* [2010] and *Machín et al.* [2010] reported that the largest northward transport of AAIW occurs from August to November, with a maximum in August and September, while the highest southward transport of MW appears in December, which is consistent with what is observed in Figure 9.

To summarize, this study discusses for the first time the influence of the Canary basin on the AMOC seasonal cycle. The winds of the Canary basin generate the formation of Rossby waves, that contribute to the seasonal cycle of the AMOC as described in *Kanzow et al.* [2010]. In addition, the AMOC seasonal behavior, as measured by the RAPID/MOCHA/WBTS project, is closely linked with the flow at the LP at both surface and intermediate layers. This study also provides with a pioneer description of the surface recirculation of the CC through the LP and shows evidence of the presence of an IPUC in the same passage.

References

Aristegui, J., P. Sangrà, S. Hernández-León, M. Cantón, A. Hernández-Guerra, and J. Kerling (1994), Island-induced eddies in the Canary Islands, *Deep Sea Res., Part I*, 41(10), 1509–1525.

Atkinson, C. P., H. L. Bryden, J. J.-M. Hirschi, and T. Kanzow (2010), On the seasonal cycles and variability of Florida Straits, Ekman and Sverdrup transports at 26°N in the Atlantic Ocean, *Ocean Sci.*, 6, 837–859.

Bakun, A., and C. S. Nelson (1991), The seasonal cycle of wind-stress curl in subtropical eastern boundary current regions, *J. Phys. Oceanogr.*, 21(12), 1815–1834.

Barton, E. (1989), The poleward undercurrent on the eastern boundary of the subtropical North Atlantic, in *Poleward Flows Along Eastern Ocean Boundaries*, edited S. J. Neshyba et al., Springer, N. Y., doi:10.1029/CE034p0082.

Belmadani, A., N. A. Maximenko, J. P. McCreary, R. Furue, O. V. Melnichenko, N. Schneider, and E. Di Lorenzo (2012), Linear wind-forced beta-plumes with application to the Hawaiian Lee Countercurrent, *J. Phys. Oceanogr.*, 43, 2071–2094, doi:10.1175/JPO-D-12-0194.1.

Calil, P. H. R., J. Kelvin, K. J. Richars, Y. Jia, and R. R. Bidigare (2008), Eddy activity in the lee of the Hawaiian Islands, *Deep Sea Res., Part II*, 55, 1179–1194.

Chidichimo, M. P., T. Kanzow, S. A. Cunningham, W. E. Johns, and J. Marotzke (2010), The contribution of eastern-boundary density variations to the Atlantic Meridional Overturning Circulation at 26.5°N, *Ocean Sci.*, 6, 475–490.

Clément, L., E. Frajka-Williams, Z. Szuts, and S. Cunningham (2014), Vertical structure of eddies and Rossby waves, and their effect on the Atlantic meridional overturning circulation at 26.5°N, *J. Geophys. Res. Oceans*, 119, 6479–6498, doi:10.1002/2014JC010146.

Comas-Rodríguez, I., A. Hernández-Guerra, E. Fraile-Nuez, A. Martínez-Marrero, V. Veníitez-Barrios, M. Pérez-Hernández, and P. Velez-Belchí (2011), The Azores Current System from a meridional section at 24.5°W, *J. Geophys. Res.*, 116, C09021, doi:10.1029/2011JC007129.

Cunningham, S. A., et al. (2007), Temporal variability of the Atlantic meridional overturning circulation at 26.5°N, *Science*, 317(5840), 935–938.

Dee, D., et al. (2011), The era-interim reanalysis: Configuration and performance of the data assimilation system, *Q. J. R. Meteorol. Soc.*, 137(656), 553–597.

Desbiolles, F., B. Blanke, A. Bentamy, and N. Grima (2014), Origin of fine-scale wind stress curl structures in the Benguela and Canary upwelling systems, *J. Geophys. Res. Oceans*, 119, 7931–7948, doi:10.1002/2014JC010015.

Duchez, A., E. Frajka-Williams, N. Castro, J.-J. Hirschi, and A. Coward (2013), Seasonal to interannual variability in density around the Canary Islands and their influence on the Atlantic Meridional Overturning circulation at 26.5°N, *J. Geophys. Res. Oceans*, 119, 1843–1860, doi:10.1002/2013JC009416.

Fraile-Nuez, E., F. Machín, P. Vélez-Belchí, F. López-Laatzen, R. Borges, V. Benítez-Barrios, and A. Hernández-Guerra (2010), Nine years of mass transport data in the eastern boundary of the North Atlantic Subtropical Gyre, *J.Geophys. Res.*, 115, C09009, doi:10.1029/2010JC006161.

Hernández-Guerra, A., J. Arístegui, M. Cantón, and L. Nykjaer (1993), Phytoplankton pigment patterns in the Canary Islands area as determined using Coastal Zone Colour Scanner data, *Int. J. Remote Sens.*, 14(7), 1431–1437.

Hernández-Guerra, A., F. López Laatzen, F. Machín, D. De Armas, and J. Pelegrí (2001), Water masses, circulation and transport in the eastern boundary current of the North Atlantic subtropical gyre, *Sci. Mar.*, 65(1), 177−186.

Hernández-Guerra, A., et al. (2002), Temporal variability of mass transport in the Canary Current, *Deep Sea Res., Part II*, 49(17), 3415–3426.

Hernández-Guerra, A., E. Fraile-Nuez, R. Borges, F. López-Laatzen, P. Vélez-Belchí, G. Parrilla, and T. J. Müller (2003), Transport variability in the Lanzarote passage (eastern boundary current of the North Atlantic subtropical Gyre), *Deep Sea Res., Part I*, 50(2), 189–200.

Hernández-Guerra, A., E. Fraile-Nuez, F. Lopeź-Laatzen, A. Martínez, G. Parrilla, and P. Velez-Belchí (2005), Canary Current and North Equatorial Current from an inverse model, *J. Geophys. Res.*, 110, C12019, doi:10.1029/2005JC003032.

Hirschi, J.-J., P. D. Killworth, and J. R. Blundell (2007), Subannual, seasonal, and interannual variability of the North Atlantic Meridional Overturning Circulation, *J. Phys. Oceanogr.*, 37(5), 1246–1265, doi:10.1175/JPO3049.1.

Jiménez, B., P. Sangrà, and E. Mason (2008), A numerical study of the relative importance of wind and topographic forcing on oceanic eddy shedding by tall, deep water islands, *Ocean Modell.*, 22 (3-4), 146–157.

Johns, W. E., et al. (2010), Continuous, array-based estimates of Atlantic Ocean heat transport at 26.5°N, *J. Clim.*, 24(10), 2429–2449, doi:10.1175/2010JCLI3997.1.

Kanzow, T., et al. (2010), Seasonal variability of the Atlantic Meridional Overturning Circulation at 26.5°N, *J. Clim.*, *23*(21), 5678–5698, doi: 10.1175/2010JCLI3389.1.

Knoll, M., A. Hernández-Guerra, B. Lenz, F. L. Laatzen, F. Mach in, T. J. Müller, and G. Siedler (2002), The eastern boundary current system between the Canary Islands and the African coast, *Deep Sea Res., Part II*, *49*(17), 3427–3440.

Laiz, I., J. Pelegrí, F. Machín, P. Sangrà, A. Hernández-Guerra, A. Marrero-Díaz, and A. Rodríguez-Santana (2012), Eastern boundary drainage of the North Atlantic subtropical gyre, *Ocean Dyn.*, *62*(9), 1287–1310, doi:10.1007/s10236-012-0560-6.

Levitus, S. (1982), Climatological atlas of the world ocean, *NOAA Prof. Pap.*, *13*, 173 pp.

Longworth, H. R., H. L. Bryden, and M. O. Baringer (2011), Historical variability in Atlantic meridional baroclinic transport at 26.5°N from boundary dynamic height observations, *Deep Sea Res., Part II*, *58*, 1754–1767.

Lumpkin, R., and P. Flament (2013), Extent and energetics of the Hawaiian Lee Countercurrent, *Oceanography*, *26*(1), 58–65, doi:10.5670/oceanog.2013.05.

Machín, F., and J. Pelegrí (2009), Northward penetration of Antarctic intermediate water off Northwest Africa, *J. Phys. Oceanogr.*, *39*(3), 512–535.

Machín, F., and J. L. Pelegrí (2006), Effect of the Canary Islands in the blockage and mixing of the North Atlantic eastern water masses, *Geophys. Res. Lett.*, *33*, L04605, doi:10.1029/2005GL025048.

Machín, F., A. Hernández-Guerra, and J. Pelegrí (2006), Mass fluxes in the Canary Basin, *Prog. Oceanogr.*, *70*(2-4), 416–447.

Machín, F., J. Pelegrí, P. Velez-Belchí, F. Lopeź-Laatzen, and A. Hernández-Guerra (2010), Seasonal flow reversals of intermediate waters in the Canary Current System East of the Canary Islands, *J. Phys. Oceanogr.*, *40*, 1902–1909.

Mason, E., F. Colas, J. Molemaker, A. Shchepetkin, C. Troupin, J. McWilliams, and P. Sangrà (2011), Seasonal variability of the Canary Current: A numerical study, *J. Geophys. Res.*, *116*, C06001, doi:10.1029/2010JC006665.

McCarthy, G., E. Frajka-Williams, W. E. Johns, M. O. Baringer, C. Meinen, H. Bryden, D. Rayner, A. Duchez, and S. A. Cunningham (2012), Observed interannual variability of the Atlantic Meridional Overturning Circulation at 26.5°N, *Geophys. Res. Lett.*, *39*, L19609, doi: 10.1029/2012GL052933.

McCarthy, G. D., D. Smeed, W. E. Johns, E. Frajka-Williams, B. I. Moat, D. Rayner, M. O. Baringer, C. Meinen, J. Collins, and H. L. Bryden (2015), Measuring the Atlantic Meridional Overturning Circulation at 26°N, *Prog. Oceanogr.*, *130*, 91–111.

McPhaden, M. J., et al. (2010), The global tropical moored buoy array, OceanObs09 Community White Paper, Venice, Italy. [Available at http://www.oceanobs09.net/proceedings/cwp/McPhaden-OceanObs09.cwp.61.pdf.]

Meinen, C. S., M. O. Baringer, and R. F. Garcia (2010), Florida current transport variability: An analysis of annual and longer-period signals, *Deep Sea Res., Part I*, *57*(7), 835–846.

Mielke, C., E. Frajka-Williams, and J. Baehr (2013), Observed and simulated variability of the AMOC at 26°N and 41°N, *Geophys. Res. Lett.*, *40*, 1159–1164, doi:10.1002/grl.50233.

Mittelstaedt, E. (1983), The upwelling area off northwest Africa––A description of phenomena related to coastal upwelling, *Prog. Oceanogr.*, *12*(3), 307–331.

Mittelstaedt, E. (1991), The ocean boundary along the northwest African coast: Circulation and oceanographic properties at the sea surface, *Prog. Oceanogr.*, *26*(4), 307–355, doi:10.1016/0079-6611(91)90011-A.

Osychny, V., and P. Cornillon (2004), Properties of Rossby waves in the North Atlantic estimated from satellite data, *J. Phys. Oceanogr.*, *34*(1), 61–76, doi:10.1175/1520-0485(2004)034<0061:PORWIT>2.0.CO;2.

Pacheco, M. M., and A. Hernandez-Guerra (1999), Seasonal variability of recurrent phytoplankton pigment patterns in the Canary Islands area, *Int. J. Remote Sens.*, *20*(7), 1405–1418.

Pelegrí, J., P. Sangrà, and A. Hernández-Guerra (1997), Heat gain in the eastern north Atlantic subtropical gyre, in *The Mathematics of Models for Climatology and Environment*, edited by J. I. Díaz, pp. 419–436, NATO ASI Series, Springer.

Pelegrí, J., J. Arístegui, L. Cana, M. González-Dávila, A. Hernández-Guerra, S. Hernández-León, A. Marrero-Díaz, M. Montero, P. Sangrà, and M. Santana-Casiano (2005), Coupling between the open ocean and the coastal upwelling region off northwest Africa: Water recirculation and offshore pumping of organic matter, *J. Mar. Syst.*, *54*(1), 3–37.

Pérez-Hernández, M. D., A. Hernández-Guerra, E. Fraile-Nuez, I. Comas-Rodríguez, V. M. Benítez-Barrios, J. Domínguez-Yanes, P. Vélez-Belchí, and D. Armas (2013), The source of the Canary Current in Fall 2009, *J. Geophys. Res. Oceans*, *118*, 2874–2891, doi:10.1002/jgrc.20227.

Piedeleu, M., P. Sangrà, A. Sánchez-Vidal, C. Fabrés, C. Gordo, and A. Calafat (2009), An observational study of oceanic eddy generation mechanisms by tall deep-water islands (Gran Canaria), *Geophys. Res. Lett.*, *36*, L14605, doi:10.1029/2008GL037010.

Risien, C., and D. Chelton (2008), A global climatology of surface wind and wind stress fields from eight years of Quik-SCAT scatterometer data, *J. Phys. Oceanogr.*, *38*, 2379–2913.

Sangrà, P., et al. (2009), The Canary Eddy Corridor: A major pathway for long-lived eddies in the subtropical North Atlantic, *Deep Sea Res., Part I*, *56*(12), 2100–2114.

Siedler, G., and M. Finke (1993), Long-period transport changes in the eastern north atlantic and their simulation by propagating waves, *J. Geophys. Res.*, *98*(C2), 2393–2406, doi:10.1029/92JC02122.

Smeed, D., et al. (2013), Observed decline of the Atlantic meridional overturning circulation 2004 to 2012, *Ocean Sci. Discuss.*, *10*(5), 1619–1645.

Sturges, W., and B. Hong (1994), Wind forcing of the Atlantic thermohaline along 32°N at low frequencies, *J. Phys. Oceanogr.*, *25*, 1706–1715.

Vélez-Belchí, P., M. González, M. D. Pérez-Hernández, and A. Hernández-Guerra (2015), Internannual, interdecadal and long-term variability. Open Ocean Temperature and salinity trends in the Canary Current large marine ecosystem, in *Oceanographic and Biological Features in the Canary Current Large Marine Ecosystem, Tech. Ser. 115*, edited by L. Valdés and I. Déniz-González, pp. 299–308, United Nations Educational, Scientific and Cultural Organization (UNESCO), Intergovernmental Oceanographic Commision, Instituto Español de Oceanografía.

Xie, S.-P., W. T. Liu, Q. Liu, and M. Nonaka (2001),Far-reaching effects of the Hawaiian Islands on the Pacific Ocean-Atmosphere System, *Science*, *292*, 2057, doi:10.1126/science.1059781.

Yang, J. (2015), Local and remote wind stress forcing of the seasonal variability of the Atlantic Meridional Overturning Circulation (AMOC) transport at 26.5°N, *J. Geophys. Res. Oceans*, *120*, 2488–2503, doi:10.1002/2014JC010317.

Zhao, J., and W. Johns (2014), Wind-driven seasonal cycle of the Atlantic Meridional Overturning Circulation, *J. Phys. Oceanogr.*, *44*(6), 1541–1562.